A New Approach to Modeling Liquid Crystal Elastomers Using Phase Field Methods

W. S. Oates[1] and H. Wang[2]

Florida Center for Advanced Aero-Propulsion–FCAAP, Department of Mechanical Engineering, Florida A & M and Florida State University, Tallahassee, FL 32310

E-mail: woates@eng.fsu.edu[1], hongbo@eng.fsu.edu[2]

Abstract.

A phase field modeling framework is developed to quantify domain structure evolution in nematic phase liquid crystal elastomers. A hyperelastic energy function is combined with liquid crystal energy relations to formulate a constitutive model for liquid crystal elastomers that undergo thermo-mechanical loads and finite deformation. A set of balance laws and constitutive relations are defined which lead to coupling behavior when finite deformation is introduced within the energy description. The theoretical framework is implemented numerically using a nonlinear finite element phase field modeling approach which couples deformation of the elastomer network with microscopic liquid crystal domain structure evolution. A comparison of monodomain and polydomain behavior is analyzed to illustrate spontaneous deformation and polydomain evolution during heating and mechanical stretching. Many of the essential constitutive relations governing these materials are obtained without the use of explicit phenomenological coupling between the liquid crystals and host elastomer.

Submitted to: *Modelling Simul. Mater. Sci. Eng.*

1. Introduction

Liquid crystals elastomers are a fascinating class of materials that combine the unusual properties of liquid crystals (Bruce et al. 2006, P. de Gennes & Prost 1993) with large deformation of a weakly cross-linked polymer. This combination of material characteristics offers exciting possibilities for developing active material systems for applications such as information storage (Viswanathan et al. 1999), lasing (Finkelmann et al. 2001, Palffy-Muhoray et al. 2006, Mayer & Zentel 2002), robotics (Ikeda et al. 2007), and biomedical devices (Woltman et al. 2007). The early synthesis research demonstrated extraordinary shape memory properties and unparalleled elastic anisotropy (Nishikawa & Finkelmann 1997, Acharya et al. 2004, Warner & Terentjev 2007). Other interesting field-coupled material properties have now emerged including electrostriction (Lehmann et al. 2001, Spillman et al. 2007), flexoelectricity (Harden et al. 2006), and photomechanical coupling (Ikeda et al. 2007, Koerner et al. 2008, Harris et al. 2005). These field-coupled characteristics provide a number of tantalizing opportunities to create a broad range of adaptable structures for advanced morphing structures, energy harvesting, drug delivery, biomimetic material systems, and novel electro-optics for information storage.

The effective utilization of liquid crystal elastomers requires a strong understanding of the underlying anisotropic liquid crystal structure, coupling with the elastomer network, and changes in material state from external effects (e.g., stress, heat, electric fields, light, etc.). Liquid crystals self-assemble into different phases with orientational order and positional ordering in smectic compositions; see (P. de Gennes & Prost 1993, Warner & Terentjev 2007, Virga 1994) for a review. These phases are temperature dependent and contain a rich range of hierarchical structures which include regions of uniform liquid crystal molecular orientation separated by defect structures. When these materials are embedded in an elastomer, the deformation is a function of stretching the elastomer network and motion of the underlying microscopic liquid crystal domain structures. A strong understanding of these interactions requires a careful assessment of the coupling behavior so that useful work is generated from externally applied fields or alternatively, a rapid change in the internal state for optical applications. A continuum model is implemented numerically using a phase field finite element approach to quantify the liquid crystal coupled elastomer deformation. This provides a computational framework that accommodates finite deformation, liquid crystal domain structure evolution, and thermo-mechanical coupling effects between the liquid crystal domains and the host elastomer.

Modeling of liquid crystal elastomers is not new and has received considerable attention (Martinoty et al. 2004, Lubensky et al. 2002, Terentjev et al. 1996, Terentjev 1993, Warner & Kutter 2002, Fried & Sellers 2004, Adams et al. 2007, Adams & Warner 2005, Conti et al. 2002, Ennis et al. 2006) and several others. A homogenized representative volume element of the effective liquid crystal elastomer structure is

often modeled using continuum methods by coupling a neo-Hookean mechanical energy density with molecular features of liquid crystals to predict elastomer shape change as a function of liquid crystal alignment; see (Warner et al. 1988, Bladon et al. 1993, Bladon et al. 1994) for a review. A theoretical continuum framework has been presented in (Anderson et al. 1999) which includes a set of balance laws relating linear and angular momentum of the elastomer and underlying liquid crystal structures. Extensions of this model are described in (Chen & Fried 2006) where generalizations on the director gradient are given. A microstrain tensor has also been considered to couple a macroscopic deformation gradient with the liquid crystal structure; see (Fried & Sellers 2005). In addition, a number of theoretical analyses of the mechanics and physics of defects in liquid crystal elastomers can be found in (Fried & Sellers 2006, Fried & Todres 2002) with additional information specific to liquid crystal defects in (Virga 1994).

Whereas a significant amount of theory has been developed to quantify the field-coupled behavior of these materials, limited numerical models exist that can predict monodomain and polydomain liquid crystal structure evolution under large deformation. The nonlinear behavior of the liquid crystals and coupling to the elastomer network leads to significant challenges in developing accurate constitutive model predictions. Often a second order tensor, Q_{ij}, is introduced to quantify anisotropy associated with the liquid crystal director n_i (i.e., orientation of the liquid crystal mesogen). An accurate representation of the order parameter(s) in terms of anisotropy and the director places significant computational challenges due to the constraints placed on the director. For example, the director is typically constrained to have a magnitude of one everywhere in the material. This can create singularities near defects (Virga 1994). One alternative that has been numerically implemented, focused on a "coarse-grained" finite element approach to predict liquid crystal reorientation when the elastomer is mechanically loaded (Conti et al. 2002). Reasonable predictions of liquid crystal evolution was predicted from the homogenized continuum model that neglected explicit computations of polydomain evolution. Here, domain structures are explicitly modeled by implementing a thermomechanical energy function of the elastomer network together with a liquid crystal energy function that includes monodomain and polydomain effects. This provides a method to further understand the role of liquid crystal domain structure evolution during deformation of the host elastomer. Polydomain behavior is estimated by introducing a pseudo-director that combines the effect of the second order anisotropy tensor Q_{ij} and the liquid crystal director n_i into an effective order parameter or "pseudo-director". This reduced order model is considered to simplify the numerical implementation while retaining the essential material mechanisms governing these materials at the microscopic length scale. The approach naturally leads to a phase field modeling formulation which couples elastomer mechanics with polydomain liquid crystal structure evolution; see (Chen 2002, Gao & Suo 2002, Castro 2003, Yu

et al. 2005, Koslowski et al. 2002, Du & Zhu 2006, Hu & Chen 2004, Zhang & Bhattacharya 2005, Su & Landis 2007, Gruverman et al. 2008) for examples using this numerical approach. Our approach is different from most other theoretical methods since the hyperelastic and liquid crystal energy are distinguished as separate energy functions to simplify numerical implementation. The mechanics of the elastomer is coupled to the liquid crystal order parameter due to finite deformation which leads to predictions of anisotropic deformation and soft elasticity similar to experiments given in the literature.

The modeling approach is illustrated in Figure 1 where the zoomed in view of the liquid crystal and elastomer structure on the left is homogenized over a microscopic representative volume element as shown on the right. It is shown in this figure that the liquid crystals are attached to the polymer backbone in a side-chain configuration. Main chain configurations can also be synthesized (Krause et al. 2009). Each configuration, as well as different liquid crystal mesogens, may give very different constitutive responses. For example, different spacers between the liquid crystal mesogens and the polymer can significantly affect the material properties. The prediction of such behavior requires a detailed analysis of the thermodynamic potential, coupling behavior, and subcontinuum features. The phenomenological model presented here includes numerical implementation of a simplified energy function with a reduced number of parameters that allow for the prediction of some of the key features governing the microscopic behavior of nematic phase liquid crystal elastomers.

The outline of the paper is given as follows. In Section 2, a set of balance laws for the liquid crystal elastomer are summarized. An energy function is introduced to obtain a set of constitutive relations that lead to coupling between a liquid crystal

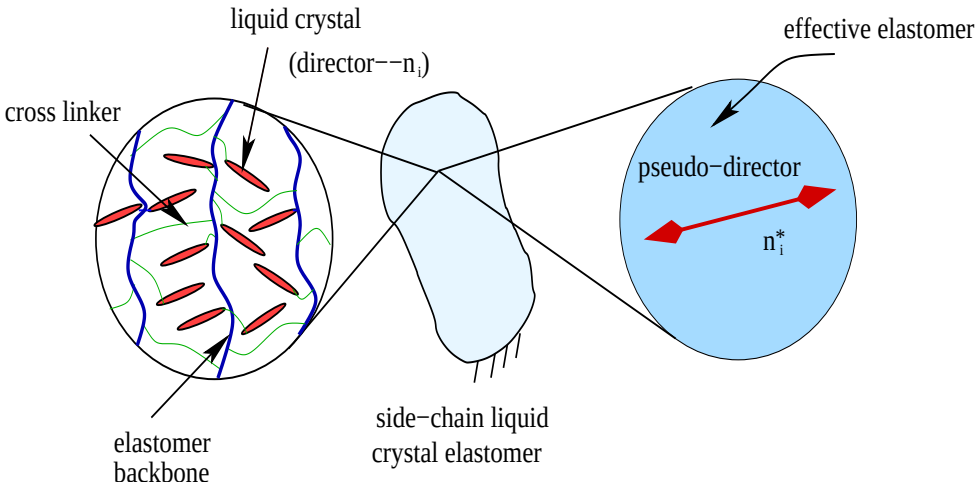

Figure 1. Schematic illustrating the homogenized model and microscale pseudo-director (n_i^*) on the right which is based on the true liquid crystal elastomer structure on the left.

pseudo-director and finite deformation of the elastomer network. In Section 3, finite element analysis is used to describe the non-equilibrium liquid crystal domain structure evolution within an elastomer network. Discussion is given in Section 4 and concluding remarks are given in Section 5.

2. Governing Equations

The thermomechanical behavior of a nonlinear solid continuum coupled to microscopic liquid crystal domain structures is formulated by introducing the balance laws and thermodynamic relations in the reference configuration. An energy function is then presented to quantify the liquid crystal elastomer constitutive behavior by using an incompressible and isotropic hyperelastic energy function in combination with monodomain and polydomain liquid crystal energetics. Relations between the reference and spatial configuration are given to describe coupling within the continuum modeling framework.

The model is formulated using the deformation gradient

$$F_{iK} = \frac{\partial x_i(\mathbf{X}, t)}{\partial X_K} \tag{1}$$

where x_i represents the current or spatial point, X_K represents the reference point, and t represents time (Malvern 1969).

It is well known that liquid crystals exhibit anisotropic constitutive behavior at temperatures below their phase transition temperature. The anisotropy is typically quantified using the second order tensor

$$Q_{ij} = \frac{Q}{2}(3n_i n_j - \delta_{ij}) \tag{2}$$

which is defined in the spatial or current domain and is limited to uniaxial behavior. The director which defines orientation of the liquid crystal mesogens is also defined in the spatial domain as n_i. The additional parameters include the Kronecker delta as δ_{ij}, and Q is a scalar parameter defining the magnitude of anisotropy. The director is defined as a unit vector with the properties $\mathbf{n} \cdot \mathbf{n} = 1$.

The introduction of Q_{ij} into an energy function requires minimization of the energy as a function of the scalar parameter Q and the director n_i as well as director gradient terms. This has been described in (Ericksen 1991) and more recently discussed by (Fried & Sellers 2006) in the context of defects and compatible strain relations. In the latter work, the scalar parameter Q was treated as a tunable parameter and distortional energy on the director was used to quantify certain strain compatibility relations near defects in the elastomer.

Here, this constraint on the director and scalar parameter is relaxed by introducing an pseudo-director that accommodates both the scalar Q and director orientation as an

effective homogenized order parameter. This pseudo-director and corresponding second order tensor are defined by

$$Q^*_{ij} = \frac{1}{2}(3n^*_i n^*_j - \delta_{ij}) \tag{3}$$

where $0 \leq |n^*_i| \leq 1$ is restricted by the form of a thermodynamic potential that will be subsequently defined by a polynomial expansion on Q^*_{ij}. It is known that ill-defined relations on n_i can occur in regions where $Q \Rightarrow 0$ under the constraint $\mathbf{n} \cdot \mathbf{n} = 1$. This is avoided by relaxing the constraint on the director such that it accommodates the key features of liquid crystal material anisotropy. The following governing equations are implemented using the pseudo-director in the force balance and thermodynamic relations. A thermodynamic potential is then given to obtain constitutive relations for numerical implementation.

2.1. Balance Laws

There is flexibility in the way the internal forces and traction along the surface may be defined when introducing an order parameter for liquid crystals within the force balance. Here, the balance law defining internal stresses due to external forces on the liquid crystal elastomer is arbitrarily decomposed into components due to stretching the elastomer network and reorientation of the microscopic liquid crystal domain structures. In this case, the force balance is defined by

$$\frac{d}{dt}\int_{\Omega_0} \rho_0 V_i dV_0 = \int_{\Gamma_0} (T^M_i + T^L_i) dS_0 + \int_{\Omega_0} \left(B^M_i + B^L_i\right) dV_0 \tag{4}$$

where Ω_0 is the volume and Γ_0 is the surface area. Both of these terms are defined from some arbitrary initial reference state. Inertial effects are included in the force balance where V_i is the effective velocity of the elastomer network and translation of the liquid crystal domains and ρ_0 is the density. The internal body force includes components due to mechanical volume forces B^M_i and the liquid crystal volume force B^L_i. The applied traction from mechanical loading is denoted by T^M_i and the traction due to the liquid crystals is denoted by T^L_i.

We assume that the liquid crystal body force can be derived from the nominal liquid crystal stress

$$B^L_i = \frac{\partial s^L_{iK}}{dX_K}. \tag{5}$$

This representation of the liquid crystal stress simplifies the introduction of certain energy functions and the corresponding constitutive relations in terms of nominal stresses. Note that this relation does not include inertial effects as defined by the separate term on the left hand side of (4).

By employing conservation of mass (Malvern 1969, Holzapfel 2000) and application of divergence theorem to the second term on the left hand side of (4), we obtain

$$\frac{\partial s_{iK}^{M}}{\partial X_K} + \frac{\partial s_{iK}^{L}}{\partial X_K} + B_i^M = \rho_0 \dot{V}_i \tag{6}$$

in the reference volume Ω_0. Note that the mechanical body force remains in the force balance which is assumed to include effects such as gravity. This form of linear momentum requires defining the total traction on the surface as

$$T_i^M + T_i^L = s_{iK}^M \hat{N}_K \tag{7}$$

where the total traction balances with mechanical forces within the material. This definition of traction illustrates the difficulty in separating the effect of forces from stretching the elastomer and rotation of the liquid crystal domains. Similar difficulties occur when decomposing mechanical stresses and stresses due to electric fields in a dielectric elastomer (McMeeking & Landis 2005). These stress components are written separately to describe the underlying liquid crystal behavior and interactions with the host elastomer as described in subsequent sections.

Now consider a force balance on the microscopic liquid crystal pseudo-director in the reference configuration

$$\int_{\Omega_0} \widetilde{\xi}_{JI}^* \hat{N}_J dV_0 = \int_{\Omega_0} \left(\widetilde{\gamma}_I^* + \widetilde{\pi}_I^*\right) dV_0 \tag{8}$$

where the director stress tensor is $\widetilde{\xi}_{IJ}^*$ and the external and intrinsic director body forces are denoted by $\widetilde{\gamma}_I^*$ and $\widetilde{\pi}_I^*$, respectively. A similar set of work conjugate relations can be found in (Rey & Denn 2002) and configurational force balance for solid-solid phase transitions in (Fried & Gurtin 1994). The liquid crystal conjugate relations between the director stress and director body forces are given in the following section. It should be noted that the internal force $\widetilde{\pi}_I^*$ includes both conservative and dissipative forces. Distinctions between the conservative and dissipative force relations are described in the following section using energy and entropy balance laws.

Again, by application of the divergence theorem on the left hand side of (8), the director force balance in the reference volume is

$$\frac{\partial \widetilde{\xi}_{JI}^*}{\partial X_J} + \widetilde{\gamma}_I^* + \widetilde{\pi}_I^* = 0 \tag{9}$$

subjected to a set of boundary conditions.

2.2. Energy Balance and Dissipative Potential Relations

The constitutive equations governing the deformation of the liquid crystal elastomer are formulated by introducing an energy description and thermodynamic balance law. According to the first law of thermodynamics, the internal energy and kinetic energy

must balance with the applied power and heat transfer rate. Here, the additional effect of the microscopic liquid crystal domain structures are included in the energy balance. Although a similar form of the energy balance can be written in the spatial form (Holzapfel 2000), the energy balance is written in the reference description to facilitate finite element implementation.

The first law states

$$\begin{aligned}\frac{d}{dt}\int_{\Omega_0}\left(\frac{1}{2}\rho_0 V_i V_i+\widetilde{u}\right)dV_0=\int_{\Omega_0}\left(B_i^M V_i+\widetilde{\gamma}_I^*\dot{\widetilde{n}}_I^*+R\right)dV_0\cdots\\ +\int_{\Gamma_0}\left(T_i^M V_i+\widetilde{\tau}_I^*\dot{\widetilde{n}}_I^*-Q_I\hat{N}_I\right)dS_0\end{aligned}\tag{10}$$

where the kinetic energy and rate of change of internal energy $\widetilde{u}$ equals external effects due to mechanical body forces and heat generation rates (R) in the volume and mechanically applied traction and the heat flux vector (Q_I) applied on the surface. The additional liquid crystal effects include ($\widetilde{\gamma}_I^*\dot{\widetilde{n}}_I^*$) applied within the volume and ($\widetilde{\tau}_I^*\dot{\widetilde{n}}_I^*$) applied on the surface. The time rate of change of the director in the reference configuration is denoted by $\dot{\widetilde{n}}_I^*$.

By use of (4), (7), and (8), a representation of the internal energy rate is obtained from (10). By assuming the result is valid for any arbitrary volume element, we have

$$\dot{\widetilde{u}}=\left(s_{iK}^M+s_{iK}^L\right)\dot{F}_{iK}-\widetilde{\pi}^*\dot{\widetilde{n}}_I^*+\widetilde{\xi}_{JI}^*\dot{\widetilde{n}}_{I,J}^*-Q_{I,I}+R\tag{11}$$

The first law relation is combined with the entropy balance to obtain a set of conjugate variables and dissipative force relations.

The second law of thermodynamics states that the rate of change of entropy is greater than or equal to the internal heat generation and heat flux according to

$$\frac{d}{dt}\int_{\Omega_0}\widetilde{s}dV_0\geq\int_{\Omega_0}\frac{R}{\Theta}dV_0-\int_{\Gamma_0}\frac{Q_I\hat{N}_I}{\Theta}dS_0\tag{12}$$

where $\widetilde{s}$ is entropy per unit reference volume, Θ is temperature, and Q_I is the heat flux in the reference frame. The local form of (12) is

$$\Theta\dot{\widetilde{s}}\geq R-Q_{I,I}+\frac{Q_I}{\Theta}\Theta_{,I}.\tag{13}$$

A Legendre transformation is introduced to obtain a Helmholtz energy density per reference volume. This thermodynamic potential is defined by $\widetilde{\psi}=\widetilde{u}-\widetilde{s}\Theta$. The time rate of change of the Helmholtz energy density is substituted into the first law relation (11). In combination with second law relation (13), we obtain

$$\dot{\widetilde{\psi}}+\widetilde{s}\dot{\Theta}\leq\left(s_{iK}^M+s_{iK}^L\right)\dot{F}_{iK}-\widetilde{\pi}^*\dot{\widetilde{n}}_I^*+\widetilde{\xi}_{JI}^*\dot{\widetilde{n}}_{I,J}^*-\frac{Q_I}{\Theta}\Theta_{,I}\tag{14}$$

A set of conjugate variables are obtained from (14) by defining the Helmholtz energy density as

$$\widetilde{\psi}=\widetilde{\psi}(F_{iK},\Theta,\widetilde{n}_I^*,\widetilde{n}_{I,J}^*)\tag{15}$$

The time rate of change of Helmholtz energy density is

$$\dot{\widetilde{\psi}} = \frac{\partial \widetilde{\psi}}{\partial F_{iK}} \dot{F}_{iK} + \frac{\partial \widetilde{\psi}}{\partial \Theta} \dot{\Theta} + \frac{\partial \widetilde{\psi}}{\partial \widetilde{n}^*_K} \dot{\widetilde{n}}^*_K + \frac{\partial \widetilde{\psi}}{\partial \widetilde{n}^*_{K,L}} \dot{\widetilde{n}}^*_{K,L} \tag{16}$$

and by substitution of this relation into (14) gives

$$\begin{aligned} &\left(s^M_{iK} + s^L_{iK} - \frac{\partial \widetilde{\psi}}{\partial F_{iK}} \right) \dot{F}_{iK} - \left(\frac{\partial \widetilde{\psi}}{\partial \widetilde{n}^*_I} + \widetilde{\pi}^*_I \right) \dot{\widetilde{n}}^*_I \cdots \\ &\quad + \left(\widetilde{\xi}^*_{JI} - \frac{\partial \widetilde{\psi}}{\partial \widetilde{n}^*_{I,J}} \right) \dot{\widetilde{n}}^*_{I,J} - \left(\widetilde{s} + \frac{\partial \widetilde{\psi}}{\partial \Theta} \right) \dot{\Theta} - \frac{Q_I}{\Theta} \Theta_{,I} \geq 0 \end{aligned} \tag{17}$$

which gives a set of conjugate variables for the thermoelastic variables

$$s_{iK} = \frac{\partial \widetilde{\psi}}{\partial F_{iK}} \quad \text{and} \quad \widetilde{s} = -\frac{\partial \widetilde{\psi}}{\partial \Theta} \tag{18}$$

where the total nominal stress is $s_{iK} = s^M_{iK} + s^L_{iK}$.

The set of conjugate variables for the liquid crystal director forces and stresses are

$$\widetilde{\eta}^*_K = \frac{\partial \widetilde{\psi}}{\partial \widetilde{n}^*_K} \quad \text{and} \quad \widetilde{\xi}^*_{KL} = \frac{\partial \widetilde{\psi}}{\partial \widetilde{n}^*_{K,L}} \tag{19}$$

where an effective liquid crystal field has been introduced as $\widetilde{\eta}^*_K$. This field only includes conservative forces. Rate dependent effects are included in the definition of $\widetilde{\pi}^*_I$

$$\widetilde{\pi}^*_I = -\widetilde{\eta}^*_I - \beta_{IJ} \dot{\widetilde{n}}^*_J \tag{20}$$

such that the inverse mobility tensor, denoted by β_{IJ}, must be positive definite according to the inequality given by (17). In addition, (17) requires the well-known heat transfer relation, $Q_I \Theta_{,I} \leq 0$.

This set of thermodynamic relations are employed in the following sections to quantify constitutive relations governing the liquid crystal elastomer material. Once the constitutive relations are quantified, the model is implemented numerically using the weak formulation to model domain structure evolution under thermo-mechanical loads via the phase field finite element model.

2.3. Liquid Crystal Behavior

It was previously discussed that a second order tensor given by (2) is often implemented to model liquid crystal anisotropy. This concept was approximated using the pseudo-director relation given by (3) and implemented here within a free energy function to quantify anisotropic deformation. The energy function is defined in the spatial domain as

$$\psi = \psi(F_{iK}, Q^*_{ij}, n^*_{i,j}) \tag{21}$$

per current volume.

A transformation to the reference domain is used to correlate changes in anisotropy as a function of the deformation gradient. The principle of virtual work is used to show that Q_{ij} is a function of deformation under transformations between the reference and spatial configurations. The transformation between the reference and spatial domain is

$$Q^*_{ij} = J^{-1} F_{iK} F_{jL} \widetilde{Q}^*_{KL} \tag{22}$$

where the Jacobian has been denoted by $J = \det(F_{iK})$ (Malvern 1969). The details of this relation are given in the Appendix. Although liquid crystal elastomers are typically incompressible (i.e., $J = 1$), this general form is used to obtain a set of stress components in the case where compressibility may occur. The model will later be restricted to incompressibility using a hyperelastic constitutive relation for the host elastomer.

A similar set of relations are defined for the pseudo-director and pseudo-director gradient. These relations follow similar arguments as given for the second order tensor Q^*_{ij} and are also given in the Appendix. The relationships between the reference and spatial configurations are

$$\begin{aligned} n^*_i &= J^{-1} F_{iK} \widetilde{n}^*_K \\ n^*_{i,j} &= J^{-1} F_{iK} F_{jL} \widetilde{n}^*_{K,L} \end{aligned} \tag{23}$$

where n^*_i and $n^*_{i,j}$ are the pseudo-director and pseudo-director gradient terms in the spatial configuration. Note that these relations are consistent with (22) and (3) where we have implied $Q^*_{ij} = 1/2(n^*_i n^*_j - n^2_s \delta_{ij})$ and $n^2_s = 1$ corresponds to the perfectly ordered director state.

The effective molecular field and director stress in each configuration are related by

$$\begin{aligned} \eta^*_i &= H_{iK} \widetilde{\eta}^*_K \\ \xi^*_{ij} &= H_{iK} H_{jL} \widetilde{\xi}^*_{KL} \end{aligned} \tag{24}$$

where H_{iK} is the inverse deformation gradient which requires $H_{iK} F_{iL} = \delta_{KL}$ and $H_{iK} F_{jK} = \delta_{ij}$ where δ_{KL} and δ_{ij} denote the Kronecker delta.

The transformation introduced here is not the only form that could be used to satisfy objectivity. The rotation tensor R_{ij}, as defined in $\mathbf{F} = \mathbf{RU}$ where $\mathbf{U}$ is the stretch tensor (Malvern 1969), is also suitable. The deformation gradient is chosen for the model since it is easier to implement mathematically although it is not as intuitive since the true director is always constrained to a magnitude of one. Regardless of the choice of R_{ij} or F_{iK}, the same set of Cauchy stress relations are obtained for the liquid crystal coupling components. For details, see application of this method on finite deforming dielectric elastomers in (McMeeking & Landis 2005, Zhao et al. 2007).

A Landau and distortional energy function per unit current volume is introduced as a function of the second order liquid crystal tensor and pseudo-director gradient

$$\psi_L = \overline{a}(\Theta) Q^*_{ii} + \frac{a(\Theta)}{2} Q^*_{ij} Q^*_{ij} + \frac{b}{3} Q^*_{ij} Q^*_{jl} Q^*_{li} + \frac{c}{4} (Q^*_{ij} Q^*_{ij})^2 + \frac{d_{ijst}}{2} n^*_{i,j} n^*_{s,t} \tag{25}$$

where the first four terms on the right hand side denote a truncated Landau energy function with phenomenological parameters $\overline{a}(\Theta)$, $a(\Theta)$, b, and c. The first two terms are assumed to be a function of temperature, Θ. The polynomial expansion on Q^*_{ij} is similar to ones in the literature (Warner & Terentjev 2007, P. de Gennes & Prost 1993), except we have included a first order term that accommodates isotropic behavior. Note that this does not violate symmetry on n^*_i since quadratic director relations are retained in the energy function (i.e., $\psi_L(n_i) = \psi_L(-n_i)$). The last term corresponds to the general form of the Frank elastic energy in terms of a fourth order tensor d_{ijst}.

The material parameters are defined as functions of the deformation gradient which is illustrated by introducing a transformation on the energy density from the spatial to reference configuration. This transformation is governed by

$$\Psi = \int_\Omega \psi dV = \int_{\Omega_0} \psi J dV_0 = \int_{\Omega_0} \widetilde{\psi} dV_0 \tag{26}$$

where ψ is the Helmholtz energy per current volume. The current volume element is dV over the domain Ω in the current configuration and dV_0 is the reference volume element over the domain Ω_0 in the reference configuration. The relation $dV = JdV_0 = \det(F_{iK})dV_0$ has also been used. These relations provide the transformation

$$\widetilde{\psi} = J\psi \tag{27}$$

In the reference configuration, the equivalent energy function is

$$\begin{aligned}\widetilde{\psi}_L = {} & \overline{a}_{KL} Q^*_{KL} + \frac{a_{KLMN}}{2} \widetilde{Q}^*_{KL} \widetilde{Q}^*_{MN} \cdots \\ & + \frac{b_{KLMNAB}}{3} \widetilde{Q}^*_{KL} \widetilde{Q}^*_{MN} \widetilde{Q}^*_{AB} \cdots \\ & + \frac{c_{KLMNABCD}}{4} \widetilde{Q}^*_{KL} \widetilde{Q}^*_{MN} \widetilde{Q}^*_{AB} \widetilde{Q}^*_{CD} + \frac{d_{KLMN}}{2} \widetilde{n}^*_{K,L} \widetilde{n}^*_{M,N}\end{aligned} \tag{28}$$

where we have defined the following parameters

$$\begin{aligned}\overline{a}_{KL}(\Theta) &= F_{iK} F_{iL} \overline{a}(\Theta) \\ a_{KLMN}(\Theta) &= J^{-1} F_{iK} F_{jL} F_{iM} F_{jN} a(\Theta) \\ b_{KLMNAB} &= J^{-2} F_{iK} F_{jL} F_{jM} F_{lN} F_{lA} F_{iB} b \\ c_{KLMNABCD} &= J^{-3} F_{iK} F_{jL} F_{iM} F_{jN} F_{iA} F_{jB} F_{iC} F_{jD} c \\ d_{KLMN} &= J^{-1} F_{iK} F_{jL} F_{sM} F_{tN} d_{ijst}\end{aligned} \tag{29}$$

For purposes of numerical implementation, the higher order tensors b_{KLMNAB} and $c_{KLMNABCD}$ were found to be unnecessary in obtaining qualitative model predictions. Higher order terms may be necessary to obtain refined model predictions in comparisons with experiments. The higher order distortional energy tensor is reduced to a scalar

parameter for approximating polydomain structure evolution of nematic phase liquid crystal behavior. The scalar parameter is

$$d_{KLMN} = \delta_{KM}\delta_{LN}K \tag{30}$$

where a single constant approximation of the Frank elastic energy has been used. In general, at least three constants are necessary to quantify splay, twist, and bend of the liquid crystal director. Here, each distortional mode is weighted equally which gives qualitative predictions of the domain structures.

Using the set of material parameters together with relations in (19), the constitutive relations for the effective liquid crystal field and liquid crystal stress tensor are

$$\begin{aligned}
\widetilde{\eta}_I^* &= \frac{\partial \widetilde{\psi}_L}{\partial \widetilde{Q}_{KL}^*}\frac{\partial \widetilde{Q}_{KL}^*}{\partial \widetilde{n}_I^*} \\
\widetilde{\eta}_I^* &= \left(\overline{a}_{KL} + a_{KLMN}\widetilde{Q}_{MN}^* + b_{KLMNAB}\widetilde{Q}_{MN}^*\widetilde{Q}_{AB}^*\right)\frac{3}{2}(\delta_{KI}\widetilde{n}_L^* + \delta_{LI}\widetilde{n}_K^*) \\
\widetilde{\xi}_{KL}^* &= K\widetilde{n}_{K,L}^*
\end{aligned} \tag{31}$$

where it should be emphasized that the phenomenological parameters are functions of the deformation gradient according to (29) which leads to liquid crystal reorientation when stretching the elastomer. These field relations can also be shown to be self-consistent in the spatial configuration using the transformations in (22)-(24) with the above energy relations in each configuration.

The additional effect of liquid crystal stress must be included in the constitutive relation due to the coupling between the material parameters and the finite deformation tensor. The nominal stress due to the liquid crystals is

$$s_{iK}^L = \frac{\partial \widetilde{\psi}_L}{\partial F_{iK}} \tag{32}$$

where coupling occurs due to the relations previously given by (29). This leads to liquid crystal stresses due to the Landau energy and Frank elastic energy.

The form of this coupling is complex and therefore only the first and second order Landau terms are given for monodomain stresses. Higher order terms are found using the same method. The temperature dependent notation on the material parameters is also dropped for brevity. The liquid crystal stresses due to first and second order Landau components are

$$\begin{aligned}
s_{rS}^{L(mono)} &= 2\overline{a}F_{rM}Q_{SM} + \frac{a}{2}J^{-1}(F_{jL}F_{rM}F_{jN} + F_{iK}F_{iM}F_{rN}\delta_{SL}\cdots \\
&\quad + F_{rK}F_{jL}F_{jN}\delta_{MS} + F_{iK}F_{rL}F_{iM}\delta_{SN})\widetilde{Q}_{KL}\widetilde{Q}_{MN}\cdots \\
&\quad - \frac{a}{2}J^{-1}H_{rS}F_{iK}F_{jL}F_{iM}F_{jN}\widetilde{Q}_{KL}\widetilde{Q}_{MN} + O(3)
\end{aligned} \tag{33}$$

where $\partial \det(\mathbf{F})/\partial F_{iK} = H_{iK} \det(\mathbf{F})$ has been applied (Holzapfel 2000). By use of the Cauchy stress relation $\sigma^L_{ji} = J^{-1} F_{jK} \dfrac{\partial \widetilde{\psi}_L}{\partial F_{iK}}$ (Malvern 1969), the liquid crystal Cauchy stress for a monodomain including the third order component is

$$\sigma^{L(mono)}_{ij} = 2\overline{a} Q_{ij} + 2a Q_{ik} Q_{jk} - \frac{a}{2} Q_{mn} Q_{mn} \delta_{ij} + 2b Q^*_{im} Q^*_{ml} Q^*_{mj} - \frac{2b}{3} Q^*_{kl} Q^*_{ln} Q^*_{nk} \delta_{ij}. \quad (34)$$

Lastly, the stresses for a polydomain material are given. In general, these stress components are

$$\begin{aligned} s^{L(d)}_{rS} &= J^{-1}(d_{rlst} F_{lL} F_{sM} F_{tN} \widetilde{n}^*_{S,L} \widetilde{n}^*_{M,N} + d_{qrst} F_{qR} F_{sM} F_{tN} \widetilde{n}^*_{R,S} \widetilde{n}^*_{M,N}) \cdots \\ &\quad - \frac{d_{qamn}}{2} J^{-1} F_{qI} F_{aJ} F_{mS} F_{nL} \widetilde{n}^*_{I,J} \widetilde{n}^*_{S,L} H_{rS} \end{aligned} \quad (35)$$

The simplified form in terms of the Cauchy stress is

$$\sigma^{L(d)}_{ij} = (d_{jlst} n^*_{i,l} + d_{ljst} n^*_{l,i}) n^*_{s,t} - \frac{d_{qrmn}}{2} n^*_{q,r} n^*_{m,n} \delta_{ij} \quad (36)$$

which simplifies further using (30).

The total liquid crystal stresses due to the pseudo-director and gradient terms are $\sigma^L_{ij} = \sigma^{L(d)}_{ij} + \sigma^{L(mono)}_{ij}$. The liquid crystal stresses are coupled with stresses due to stretching the elastomer as described in the following section.

2.4. Thermomechanical Behavior

For purposes of demonstrating field-coupled liquid crystal elastomer characteristics, the neo-Hookean hyperelastic energy function is introduced; however, a number of hyperelastic energy functions could be inserted into the thermodynamic framework to obtain a refined model prediction. A simplified model is presented here which illustrates qualitative predictions on liquid crystal domain structure coupling to the thermoelastic behavior of the host elastomer.

The neo-Hookean model is defined as a function of the first and third strain invariants. The principal stretches are λ_i for $i = 1, 2, 3$. The first and third strain invariants are $I_1 = \lambda_1^2 + \lambda_2^2 + \lambda_3^2$ and $I_3 = \lambda_1 \lambda_2 \lambda_3$, respectively. This function is combined with thermal effects as

$$\begin{aligned} \widetilde{\psi}_M(I_1, I_3, \Theta) &= \frac{\mu}{2}(I_1 - 3) - p(I_3 - 1) + \frac{p^2}{2\kappa} \cdots \\ &\quad + C_v \left[(\Theta - \Theta_0) - \Theta \log\left(\frac{\Theta}{\Theta_0}\right) \right] \end{aligned} \quad (37)$$

where μ is the shear modulus, κ is the bulk modulus, and C_v is the specific heat capacity at constant deformation (Fung 1965). Note that we have assumed incompressible material behavior where p serves as an indeterminate Lagrange multiplier.

The nominal stress can be obtained using

$$s_{iK}^{M} = 2F_{iL}\frac{\partial\widetilde{\psi}_{M}}{\partial C_{KL}} \tag{38}$$

where $C_{KL} = F_{iK}F_{iL}$ (Holzapfel 2000). Using (37), a simplified form of the nominal stress in terms of the strain invariants is

$$s_{iK}^{M} = \mu F_{iK} - pI_3F_{iK}^{-T} \tag{39}$$

see (Holzapfel 2000) for details.

The entropy change is defined by

$$\widetilde{s} = C_v \ln\left(\frac{\Theta}{\Theta_0}\right) - \overline{a}_{KL}\widetilde{Q}_{KL}^{*} - \frac{a_{KLMN}}{2}\widetilde{Q}_{KL}\widetilde{Q}_{MN} \tag{40}$$

where (18) has been applied and we have assumed linear dependence in the temperature on constants defined in (29).

The caloric equation of state governing heat transfer is formulated using Duhamel's law of heat conduction

$$Q_I = -Jk_{mn}H_{mI}H_{nJ}\Theta_{,J} \tag{41}$$

where k_{mn} is the spatial thermal conductivity coefficient. The heat transfer relations between the reference and spatial configuration are given in the Appendix.

The total change in entropy is obtained from (13) and the Helmholtz energy as

$$\Theta\dot{\widetilde{s}} = -\Theta\left(\frac{\partial^2\widetilde{\psi}}{\partial\Theta\partial\widetilde{Q}_{AB}^{*}}\frac{\partial\widetilde{Q}_{AB}^{*}}{\partial\widetilde{n}_I^{*}}\dot{\widetilde{n}}_I^{*} + \frac{\partial^2\widetilde{\psi}}{\partial\Theta^2}\dot{\Theta}\right) = R - Q_{I,I} + \frac{Q_I}{\Theta}\Theta_{,I} + \Theta\dot{\widetilde{s}}_g \tag{42}$$

where we have defined entropy production by $\widetilde{s}_g$ to include dissipative mechanisms in addition to the thermal gradient term. Note that configurational entropy changes due to the deformation gradient have been neglected. By use of the definition of specific heat ($C_v = -\Theta\dfrac{\partial^2\widetilde{\psi}}{\partial\Theta^2}$), we have

$$\begin{aligned} C_v\dot{\Theta} = R + Jk_{mn}H_{mI}H_{nJ}\Theta_{,IJ} - \frac{Jk_{mn}H_{mI}H_{nJ}\Theta_{,J}}{\Theta}\Theta_{,I}\cdots \\ +3\left(\overline{a}_{IA} + a_{IAMN}\widetilde{Q}_{MN}^{*}\right)\Theta\widetilde{n}_A^{*}\dot{\widetilde{n}}_I^{*} \end{aligned} \tag{43}$$

where the energy balance is shown to include effects due to liquid crystal motion. Note that we have neglected entropy production, $\widetilde{s}_g = 0$.

This is the energy balance in terms of temperature in the reference configuration. An equivalent form could be formulated in the spatial domain (Holzapfel 2000), but the reference configuration is used for numerical modeling. This equation is coupled with linear momentum and the liquid crystal director force balance for finite element modeling as described in the following section.

3. Model Analysis and Finite Element Implementation

The material coupling between the liquid crystal domain structures and elastomer network leads to a complex material state governed by the nonlinear equations of motion. Finite element modeling is used to predict evolution of monodomain and polydomain structures numerically. The balance equations are summarized in the weak form for numerical implementation within the finite element framework. Whereas spectral methods could also be employed, the finite element model is used so that non-periodic boundary conditions can be applied. The governing equations include linear momentum previously given by (6), the liquid crystal pseudo-director force balance (9), and the caloric equation of state governing heat transfer (43). The finite element formulation results in a form of a phase field model due to the relatively small liquid crystal distortional energy and the non-convex Landau energy description governing the liquid crystal domain structure formation. This leads to domain structures that form as the material is cooled from an initial random, high temperature state or reorient in the presence of finite deformation. Details describing how domain structure formation is modeled will be given.

3.1. Weak Formulation

The finite element model is summarized by the three sets of governing equations rewritten in the weak form. The energy balance previously given in the strong form by (43) is written in the weak form and coupled with the weak form of the force balance law (6) and pseudo-director force balance (9). The energy balance in terms of temperature rates is

$$\begin{aligned}\frac{d}{dt}\int_{\Omega_0} C_v\dot{\Theta}\zeta dV_0 &= \int_{\Omega_0}\left[Q_I\zeta_{,I}+\left(R+\frac{Q_I}{\Theta}\Theta_{,I}+a_0\Theta\widetilde{n}_I\dot{\widetilde{n}}_I\right)\zeta\right]dV_0\cdots \\ &\quad -\int_{\Gamma_0} Q_I\hat{N}_I\zeta dS_0\end{aligned} \tag{44}$$

where ζ is the weight function. The heat conduction is $k_{MN}=J^{-1}F_{iM}F_{jN}k_0\delta_{ij}$ where isotropy in the conduction tensor is assumed to hold under zero strain, but anisotropic conduction occurs as the pseudo-director evolves during cooling. The thermal material parameters include $C_v=2$ kJ/(kg K) and $k_0=0.2$ W/(m K). This equation is coupled with following weak form of the elastomer and pseudo-director force balance equations

$$\begin{aligned}&\int_{\Omega_0}\left(s^M_{iK}+s^L_{iK}\right)\frac{\partial\zeta_i}{\partial X_K}dV_0=\int_{\Gamma_0}T^M_i\zeta_i dS_0\\ &\int_{\Omega_0}\widetilde{\xi}^*_{JI}\frac{\partial\zeta_I}{\partial X_J}dV_0=\int_{\Omega_0}\widetilde{\pi}^*_I\zeta_I dV_0+\int_{\Gamma_0}\widetilde{\tau}^*_I\zeta_I dS_0\end{aligned} \tag{45}$$

where inertial effects and body forces in $(45)_1$ are neglected. A set of weight functions, ζ_i and ζ_I, have also been introduced. Applied liquid crystal internal forces have been

set to zero ($\widetilde{\gamma}_I^* = 0$) and non-equilibrium domain structure formation is included in the definition of $\widetilde{\pi}_I$. In the numerical simulations in the following section, the pseudo-director traction will also be set to zero on all boundaries ($\widetilde{\tau}_I^* = 0$).

3.2. Monodomain Model Predictions

The model given by (44) and (45) is implemented in two dimensions on a domain of size 1×1 μm^2. The parameters used in the model are given in Table 1. Comsol 3.5 was used to implement the model since general partial differential equations can be implemented using this software. The mesh is refined uniformly over the grid space until convergence between model runs is achieved. A mesh of 672 elements were used in the monodomain simulations described below. A GMRES solver with pre-conditioning is used to achieve converged results for each time step.

A monodomain aligned along the horizontal or equivalently, the X_1 direction is considered. The model is allowed to reach equilibrium under zero traction boundary conditions by applying initial conditions with the pseudo-director uniformly oriented in the X_1 direction. The left bottom corner point is fully mechanically constrained in combination with a roller along the bottom edge to prevent rigid body rotation. The pseudo-director value at equilibrium is 0.9. Then the model is stretched in the X_2 direction using displacement control to ensure stability during domain formation and reorientation. The boundary conditions during stretching include full constraint of the bottom edge and vertical displacement control along the top edge. Anisotropic deformation is predicted at equilibrium with a spontaneous strain of approximately 10% in the direction of the pseudo-director and contraction in the orthogonal direction. This spontaneous strain can be increased or decreased dependent on the Landau coefficients and the shear modulus. A large bulk modulus is used to ensure incompressibility. In Figure 2(a), the onset of reorientation of the domain structures is observed and in Figures 2(b,c), large reorientation occurs where the liquid crystals align with the external load. It should be noted that the displacement controlled boundary conditions stabilize the model to allow tracking of relaxation during rotation of the liquid crystal domains. The rotation of domain structures is a consequence of increased mechanical energy and coupling that occurs from finite deformation. This coupling distorts the liquid crystal Landau energy function and results in a change in liquid crystal orientation to a lower energy state. The monodomain structure originally aligned in the X_1 direction becomes unfavorable due to higher mechanical energy and therefore the monodomain reorients to align with the mechanical load.

This behavior provides insight on the concept known as soft elasticity often observed in these materials during liquid crystal reorientation. The domain pattern that forms is similar to ones given in the literature where striped domains form parallel to the loading direction (Kundler & Finkelmann 1995, Conti et al. 2002). It is important to note that the nucleation of domain structures is strongly dependent on stress concentrations near

the clamped ends in our simulations. When a roller is applied to the bottom of the model, domain reorientation occurs at a higher stretch value. The displacement boundary condition at the top may also effect these results. The boundary condition along the top edge constrains motion to only allow uniform displacements. Twinned domain structures may initiate away from the bottom edge with a force boundary condition along the top edge. The corresponding load versus stretch is plotted in Figure 3. The drop in stress near $\lambda_2 = 1.5$ corresponds to the region of large scale domain reorientation. Reasonable correlations relative to data are observed although more work is required to obtain quantitative constitutive model predictions. These results were achieved using two Landau coefficients, a single distortional constant, and shear modulus as given in Table 1.

Table 1. Parameters used in the liquid crystal elastomer finite element phase field model. A single constant was used for the inverse mobility tensor, $\beta_{IJ} = \beta_0 \delta_{IJ}$.

Parameter	Value	Unit
μ	1	kPa
κ	1	GPa
$\overline{a}$	-150	kPa
Θ_0	350	K
a	100	kPa
b	0	kPa
c	0	kPa
K	7×10^{-12}	N
β_0	2×10^{-11}	Ns/m^2

3.3. Polydomain Model Predictions

Simulations for a polydomain structure are given by slowly cooling the material while remaining near equilibrium by starting from a high temperature isotropic random state with small random perturbations on the liquid crystal pseudo-director $|\tilde{\mathbf{n}}^*| \simeq 1 \times 10^{-6}$. Once the domain structures reach equilibrium, the model is heated to illustrate how liquid crystal domain structures revert back to the isotropic state. In these simulations, we control the heating rate slowly so that each time step is close to equilibrium. The model is mechanically constrained similar to the monodomain model. The bottom layer is mechanically constrained in the vertical direction and fully constrained at the left bottom corner and otherwise allowed to freely expand. A set of domain structures are predicted as the model approaches equilibrium as shown in Figure 4. In these simulations, the mesh density was 1664 to ensure convergent predictions of polydomain structures.

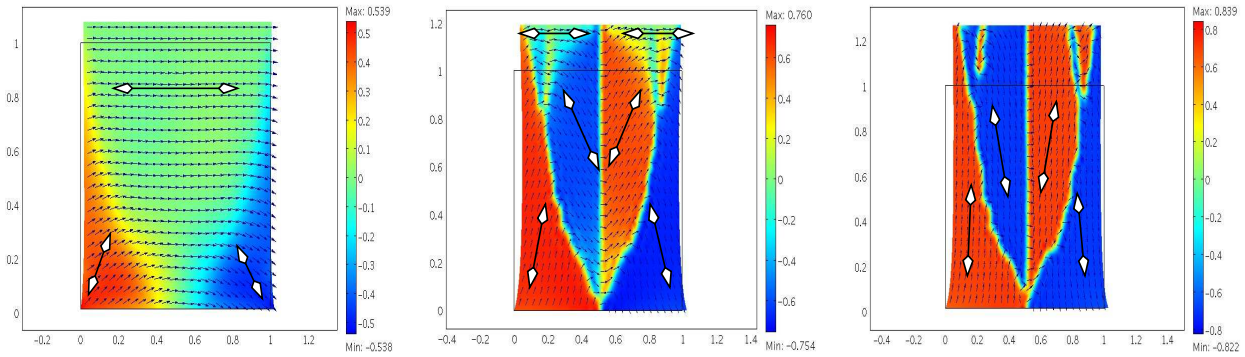

(a) (b) (c)

Figure 2. Domain structure formation from an initial monodomain during uniaxial stretching. The pseudo-director component $\widetilde{n}_2^*$ is shown. Under increasing levels of stretch, striped domains begin to form. The deformation shown is scaled down for easier visualization.

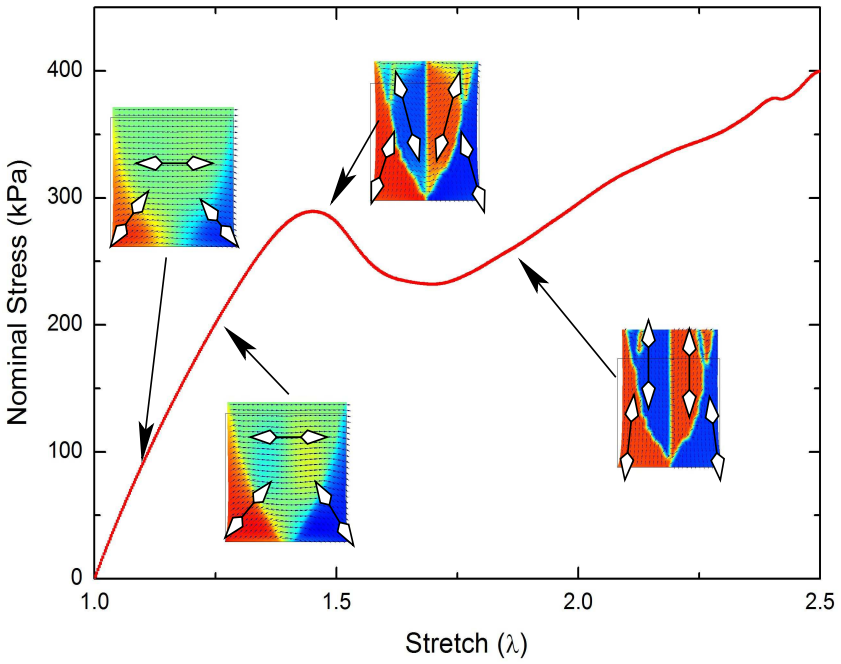

Figure 3. Plot of the stress versus stretch corresponding to the domain structure evolution in Figure 2. Note that the soft elastic region ($1.4 < \lambda < 1.8$) is strongly correlated with domain structure reorientation.

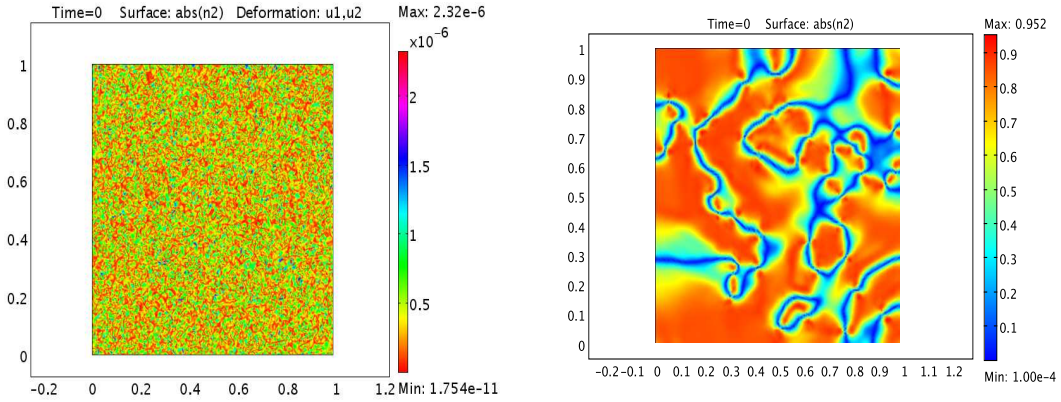

(a) (b)

Figure 4. Finite element model results comparing a set of random initial conditions on the director in the high temperature isotropic phase in (a) with equilibrium domain structures in (b). The units are in microns and the pseudo-director component $\widetilde{n}_2^*$ is plotted. The material was uniformly cooled to an equilibrium temperature of 250 K in (b).

From the nematic phase equilibrium state given in Figure 4, the model is slowly heated above the isotropic phase transition temperature. Results at 325 K and 370 K are illustrated in Figure 5. The original domain structures broaden and the domain structures begin to merge together as the material approaches the phase transition temperature Θ_0. It should be noted that thermal expansion on the host elastomer has been neglected. The introduction of thermal deformation of the elastomer network could play an inverse role on the domain structure evolution that was predicted by the model.

4. Discussion

A theoretical framework describing interactions between liquid crystal domains and deformation of an elastomer network has been described and implemented numerically. A pseudo-director was introduced to approximate the effect of anisotropy within a second order tensor Q_{ij}^*. This modeling framework results in a reduced-order model that accommodates the conventional scalar parameter Q and liquid crystal director n_i that is often used to describe liquid crystals. Whereas more refined models could be developed by treating these terms as independent variables, the results illustrate that many of the essential features governing these materials can be predicted by using conventional hyperelastic and liquid crystal energy functions coupled to geometric nonlinearities.

Liquid crystal domain structure coupling to the deformation of the host elastomer was quantified by including finite deformation in the energy description and balance equations. A rotational invariant pseudo-director ($\widetilde{n}_i^*$) and second order liquid

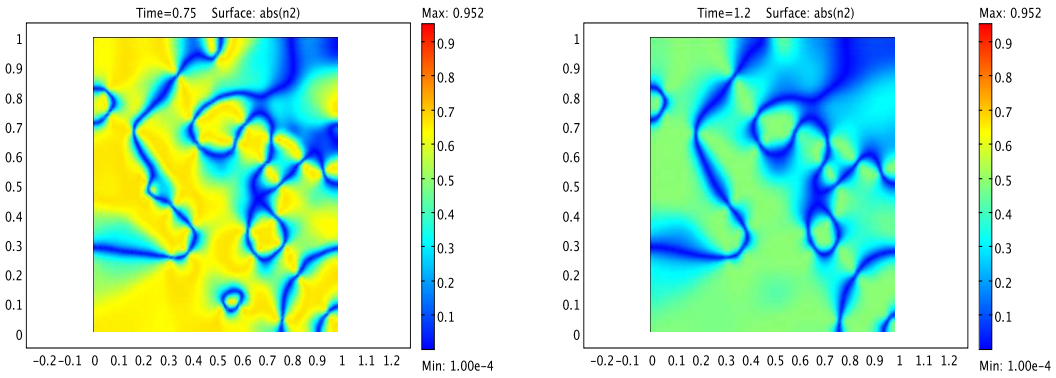

(a) (b)

Figure 5. From the equilibrium configuration in Figure 4(b), the model is heated slowly to allow for a uniform temperature distribution. The instantaneous temperature is 325 K in (a) and 370 K in (b). Again, the pseudo-director component $\widetilde{n}_2^*$ is plotted.

crystal tensor $\widetilde{Q}_{ij}^*$ was introduced in the energy function in terms of the deformation gradient. A similar form could have been implemented using the rotation tensor, although the resulting field-coupled stresses have been shown to be identical (Zhao et al. 2007, McMeeking & Landis 2005). While the pseudo-director induced deformation is similar to electric field-coupled stresses in dielectric elastomers, liquid crystal coupling to the elastomer is more complex. This is due to the nonconvex liquid crystal energy function that is modeled by introducing higher order anisotropic effects. The anisotropy in the energy function leads to deformation that is dependent on the orientation of the pseudo-director. Moreover, an additional set of stress relations due to polydomain structures have been defined using this approach.

Polydomain effects were included in the model using Frank elastic energy based on first order gradients on the pseudo-director. Numerical modeling was limited to the single constant Frank elastic energy approximation which assumes penalties due to splay, twist, and bend are equal. This gives a qualitative estimate on the domain structure formation since each distortional mode is known to vary. The single constant approximation was used to simplify the constitutive model implementation since this approximation results in symmetric liquid crystal stress components in a polydomain configuration. When the three Frank elastic energy parameters are not equal ($K_1 \neq K_2 \neq K_3$), special requirements must be introduced to ensure angular momentum is satisfied. The angular momentum relation results in internal moments that must balance with the pseudo-director forces so that angular momentum is satisfied. These relations will be numerically implemented in a future manuscript for the more general three constant Frank elastic energy model.

The theoretical model was numerically implemented and comparisons between

monodomain and polydomain configurations were quantified. It was shown that the Landau parameters are functions of the deformation gradient when transformations between the spatial and reference configurations are introduced. This leads to spontaneous deformation and reorientation of the pseudo-director without introducing phenomenological coupling coefficients. The model parameters used here result in spontaneous strain on the order of 10%; larger values will be considered in future work to obtain quantitative predictions with experimental results. Although only qualitative predictions have been considered, it has been shown that finite deformation coupling provides an insight into soft elasticity. As shown in Figure 2 and the corresponding stress versus stretch plot in Figure 3, insight on the behavior of liquid crystal domain structure evolution and nonlinear mechanics is predicted by using a relatively simple hyperelastic energy function and a classic liquid crystal energy function. More work is required to obtain quantitative model predictions by reviewing the existing parameters and rate effects which may change the peak stress during reorientation. However, the results are similar to predictions given by (Conti et al. 2002), but explicit tracking of monodomain to polydomain transitions has been included in the present model.

Several model predictions of polydomain configurations were given. From a high temperature pseudo-random state, equilibrium domain structures were simulated down to a temperature 100 K below the phase transition temperature $\Theta_0 = 350$ K. It should also be noted that the model was slowly heated and cooled to avoid uncertainties in thermal transport rates. The model predicted domain structures with a size on the order of 200-400 nm. In addition, the coherence length based on $\xi_N = \sqrt{-K/\overline{a}}$ gave a length of 7 nm using values in Table 1 which is reasonable for liquid crystals (Warner & Terentjev 2007). It should be noted that a thorough study of the distortional energy constants and coupling with the Landau coefficients and hyperelastic energy has not been done. Refined domains are expected to occur in regions of larger stress which may play an important role in domain structure equilibrium sizes and evolution under external loading.

5. Concluding Remarks

A microscale model for liquid crystal elastomers was numerically implemented using a finite element phase field approach to predict domain structure evolution. Finite deformation was included in the energy description to quantify the effect of elastomer deformation due to microscopic liquid crystal pseudo-director forces. Estimates on spontaneous strain and domain structure evolution from external loads were predicted for a monodomain using simplified Landau and distortional energy functions. The additional effect of Frank elastic energy was shown to lead to domain structure formation in the case of large stretching and temperature changes. The method provides a simplified approach to modeling the complex behavior of these materials. Current work is focused on quantitative model predictions and unusual coupling behavior with light

in photoactive liquid crystal elastomer networks.

Acknowledgments

The authors gratefully acknowledges support from the Florida Center for Advanced Aero-Propulsion (FCAAP) and a summer faculty ASEE program with Eglin Air Force Research Laboratory.

6. Appendix

Spatial and reference relations for the effective liquid crystal molecular fields and tensor relations are given here. Test functions are introduced to quantify these terms following a similar approach given in (Suo et al. 2008). Additional terms on the pseudo-director gradient are also presented.

6.1. Effective Molecular Field Relations

A set of conjugate variable relations were defined for the liquid crystal energy relations as given by (19). We use methods of virtual work to determine a set of relations between the spatial and reference configuration starting with η_i^* and ξ_{ij}^*. We then use similar arguments to obtain relations for Q_{ij}^* based on (22).

By definition, we have a change in the energy of a monodomain liquid crystal volume element given by

$$\eta_i^* \delta n_i^* dV = \widetilde{\eta}_K^* \delta \widetilde{n}_K^* dV_0 \tag{46}$$

where dV is a volume element in the current configuration, dV_0 is a volume element in the reference configuration, and δn_i^* and $\delta \widetilde{n}_K^*$ are variations in the orientation of the pseudo-director in the spatial and reference configuration, respectively. By introduction of an arbitrary test function ζ for the effective molecular fields η_i^* and $\widetilde{\eta}_K^*$, we have

$$\frac{\partial \zeta}{\partial x_i} \delta n_i^* dV = \frac{\partial \zeta}{\partial X_K} \delta \widetilde{n}_K^* dV_0. \tag{47}$$

We use the relation on the test function

$$\frac{\partial \zeta}{\partial X_K} = \frac{\partial \zeta}{\partial x_i} \frac{\partial x_i}{\partial X_K} = \frac{\partial \zeta}{\partial x_i} F_{iK} \tag{48}$$

and by the use of the spatial and reference volume element relations, we have

$$dV = J dV_0 \tag{49}$$

where the determinant of the deformation gradient was previously defined by $J = \det(F_{iK})$. This provides

$$\delta n_i^* = J^{-1} F_{iK} \delta \widetilde{n}_K^* \tag{50}$$

and since the variation denoted by δ is arbitrary, this leads to $(23)_1$.

Similarly, if we take

$$\widetilde{\eta}_K^* = \frac{\partial \zeta}{\partial X_K} \quad \text{and} \quad \eta_i^* = \frac{\partial \zeta}{\partial x_i} \tag{51}$$

we have

$$\eta_i^* = \frac{\partial \zeta}{\partial X_K}\frac{\partial X_K}{\partial x_i} = \widetilde{\eta}_K^* H_{iK}. \tag{52}$$

which gives $(24)_1$.

6.2. Liquid Crystal Director Gradient Relations

Variations in the energy for the liquid crystal director gradient are defined by

$$\left(\xi_{ij}^{s,*}\delta n_{ij}^{s,*} + \xi_{ij}^{a,*}\delta n_{ij}^{a,*}\right) dV = \left(\widetilde{\xi}_{KL}^{s,*}\delta \widetilde{n}_{KL}^{s,*} + \widetilde{\xi}_{KL}^{a,*}\delta \widetilde{n}_{KL}^{a,*}\right) dV_0 \tag{53}$$

where the field components have been decomposed into symmetric and anti-symmetric components denoted by superscript s and a, respectively. The terms $\xi_{ij}^{s,*}$ and $n_{ij}^{s,*}$ are defined in the current volume element dV. Similar terms are defined in the reference configuration as $\widetilde{\xi}_{KL}^{s,*}$, $\widetilde{n}_{KL}^{s,*}$, $\widetilde{\xi}_{KL}^{a,*}$, and $\widetilde{n}_{KL}^{a,*}$ which are defined over the reference volume element dV_0. Note that cross terms such as $n_{ij}^{s,*}\xi_{ij}^{a,*}$ are zero and have been omitted.

The second order tensors $\delta n_{ij}^{s,*}$ and $\delta n_{ij}^{a,*}$ are

$$\delta n_{ij}^{s,*} = \frac{1}{2}\left(\delta n_{i,j}^* + \delta n_{j,i}^*\right) \quad \text{and,} \quad \delta n_{ij}^{a,*} = \frac{1}{2}\left(\delta n_{i,j}^* - \delta n_{j,i}^*\right) \tag{54}$$

which gives $\delta n_{i,j}^* = \delta n_{ij}^{s,*} + \delta n_{ij}^{a,*}$ and similarly

$$\xi_{ij}^{s,*} = \frac{1}{2}\left(\xi_{ij}^* + \xi_{ji}^*\right) \quad \text{and,} \quad \xi_{ij}^{a,*} = \frac{1}{2}\left(\xi_{ij}^* - \xi_{ji}^*\right) \tag{55}$$

An equivalent set of relations are used in the reference configuration.

Based on (53), a test function β_i is introduced for the tensor relations in (55)

$$\xi_{ij}^{s,*} = \frac{1}{2}\left(\frac{\partial \beta_i}{\partial X_K}\frac{\partial X_K}{\partial x_j} + \frac{\partial \beta_j}{\partial X_L}\frac{\partial X_L}{\partial x_i}\right) = \frac{1}{2}\left(\frac{\partial \beta_i}{\partial X_K}H_{jK} + \frac{\partial \beta_j}{\partial X_L}H_{iL}\right) \tag{56}$$

we further reduce this relation by introducing a scalar function ϕ and let

$$\beta_i = \frac{\partial \phi}{\partial x_i} \quad \text{and} \quad \beta_i = \frac{\partial \phi}{\partial X_K}\frac{\partial X_K}{\partial x_i} = \widetilde{\beta}_K H_{iK} \tag{57}$$

By substitution of $(57)_2$ into (56) we have

$$\xi_{ij}^{s,*} = \frac{1}{2}\left(\frac{\partial}{\partial X_K}\left(\widetilde{\beta}_L H_{iL}\right)H_{jK} + \frac{\partial}{\partial X_L}\left(\widetilde{\beta}_K H_{jK}\right)H_{iL}\right) \tag{58}$$

Since $\xi_{ij}^{s,*} = \xi_{ji}^{s,*}$ and $\dfrac{\partial H_{iL}}{\partial X_K} = \dfrac{\partial^2 X_L}{\partial X_K \partial x_i} = 0$, (58) simplifies to

$$\xi_{ij}^{s,*} = \frac{1}{2}\left(\widetilde{\beta}_{K,L} + \widetilde{\beta}_{K,L}\right) H_{iL} H_{jK} \tag{59}$$

The anti-symmetric term is obtained in a similar manner. Starting with

$$\xi_{ij}^{a,*} = \frac{1}{2}\left(\frac{\partial \beta_i}{\partial X_K}\frac{\partial X_K}{\partial x_j} - \frac{\partial \beta_j}{\partial X_L}\frac{\partial X_L}{\partial x_i}\right) = \frac{1}{2}\left(\frac{\partial \beta_i}{\partial X_K} H_{jK} - \frac{\partial \beta_j}{\partial X_L} H_{iL}\right) \tag{60}$$

the anti-symmetric tensor simplifies to

$$\xi_{ij}^{a,*} = \frac{1}{2}\left(\widetilde{\beta}_{L,K} - \widetilde{\beta}_{K,L}\right) H_{iL} H_{jK} \tag{61}$$

where $(57)_2$ has been substituted into (60). The final relation is given by

$$\xi_{ij}^{*} = \xi_{ij}^{s,*} + \xi_{ij}^{a,*} = \left(\widetilde{\xi}_{KL}^{s,*} + \widetilde{\xi}_{KL}^{a,*}\right) H_{iL} H_{jK} = \widetilde{\xi}_{KL}^{*} H_{iL} H_{jK} \tag{62}$$

which is equivalent to $(24)_2$.

The director gradient in the reference and spatial configurations are defined by substitution of (62) and (49) into (53). The symmetric component of the director is

$$\delta n_{ij}^{s,*} \widetilde{\xi}_{KL}^{s,*} J H_{iK} H_{jL} dV_0 = \delta \widetilde{n}_{KL}^{s,*} \widetilde{\xi}_{KL}^{s,*} dV_0 \tag{63}$$

which gives

$$\delta n_{ij}^{s,*} = J^{-1} F_{iK} F_{jL} \delta \widetilde{n}_{KL}^{s,*} \tag{64}$$

and similarly for the anti-symmetric component

$$\delta n_{ij}^{a,*} = J^{-1} F_{iK} F_{jL} \delta \widetilde{n}_{KL}^{a,*} \tag{65}$$

such that

$$\delta n_{i,j}^{*} = J^{-1} F_{iK} F_{jL} \left(\delta \widetilde{n}_{KL}^{s,*} + \delta \widetilde{n}_{KL}^{a,*}\right) = J^{-1} F_{iK} F_{jL} \delta \widetilde{n}_{K,L}^{*} \tag{66}$$

It can be shown that a similar set of relations can be obtained for the second order tensor Q_{ij}^{*} and $\widetilde{Q}_{KL}^{*}$ by defining a conjugate second order tensor for Q_{ij}^{*}. Virtual changes in the energy lead to (22).

6.3. Heat Transfer Relations

The relations defining the heat flux vector Q_I are given here. The difference in heat transfer in the reference and spatial configurations is

$$Q_I = JH_{jI}q_j \tag{67}$$

where H_{jI} is the inverse deformation gradient and q_i is the heat flux in the spatial configuration. The heat transfer constitutive relation in the spatial configuration is

$$q_i = -k_{ij}\Theta_j = -k_{ij}H_{jK}\Theta_{,K} \tag{68}$$

where the relation

$$\Theta_{,j} = H_{jK}\Theta_{,K} \tag{69}$$

has been applied. By application of (67) and (68), the previous relation given by (41) is obtained.

References

Acharya B, Primak A & Kumar S 2004 *Phys. Rev. Lett.* **92**(14), 145506–1–145506–4.
Adams J, Conti S & DeSimone A 2007 *Continuum Mech. Thermodyn.* **18**, 319–334.
Adams J & Warner M 2005 *Phys. Rev. E* **71**, 021708–1–021708–15.
Anderson D, Carlson D & Fried E 1999 *J. Elasticity* **56**, 33–56.
Bladon P, Terentjev E M & Warner M 1993 *Phys. Rev. E* **47**(6), R3838–R3840.
Bladon P, Warner M & Terentjev E M 1994 *Macromolecules* **27**(24), 7067–7075.
Bruce D, Goodby J, Sambles J & Coles H 2006 *Phil. Trans. R. Soc. A* **364**, 2567–2571.
Castro M 2003 *Phys. Rev. B* **67**, 035412–1–035412–8.
Chen L 2002 *Annu. Rev. Mater. Res.* **32**, 113–140.
Chen Y C & Fried E 2006 *Proc. Roy. Soc. A* **462**, 1295–1314.
Conti S, DeSimone A & Dolzmann G 2002 *J. Mech. Phys. Solids* **50**, 1431–1451.
Du Q & Zhu L 2006 *J. Comput. Math.* **24**(3), 265–280.
Ennis R, Malacarne L, Palffy-Muhoray P & Shelley M 2006 *Phys. Rev. E* **74**, 061802–1–061802–8.
Ericksen J 1991 *Arch. Rational Mech. Anal.* **113**, 97–120.
Finkelmann H, Kim S, Muñoz A & Palffy-Muhoray P 2001 *Adv. Mater.* **13**(14), 1069–1072.
Fried E & Gurtin M 1994 *Physica D* **72**, 287–308.
Fried E & Sellers S 2004 *J. Mech. Phys. Solids* **52**, 1671–1689.
Fried E & Sellers S 2005 *J. Chem. Phys.* **123**, 044901.
Fried E & Sellers S 2006 *J. Chem. Phys.* **124**, 024908.
Fried E & Todres R 2002 *J. Polymer Sci. B: Polymer Physics* **40**(18), 2098–2106.
Fung Y 1965 *Foundations of Solid Mechanics* Prentice-Hall, Inc. Englewood Cliffs, NJ.
Gao Y & Suo Z 2002 *ASME J. Appl. Mech.* **69**, 419–424.
Gruverman A, Cross J & Oates W 2008 *Appl. Phys. Lett.* **93**, 242902.
Harden J, Mbanga B, Éber N, Fodor-Csorba K, Sprunt S, Gleeson J & Jákli A 2006 *Phys. Rev. Lett.* **97**, 157802–1–157802–4.
Harris K, Cuypers R, Scheibe P, van Oosten C, Bastiaansen C, Lub J & Broer D 2005 *J. Mater. Chem.* **15**, 5043–5048.
Holzapfel G 2000 *Nonlinear Solid Mechanics* John Wiley & Sons, Inc. Chichester.

Hu H L & Chen L 2004 *Acta. Mater.* **52**(3), 749–764.
Ikeda T, Mamiya J & Yu Y 2007 *Angew. Chem.* **46**, 506–528.
Koerner H, White T, Tabirya N, Bunning T & Vaia R 2008 *Materials Today* **11**(7–8), 34–42.
Koslowski M, Cuitiño A & Ortiz M 2002 *J. Mech. Phys. Solids* **50**, 2597–2635.
Krause S, Zander F, Bergmann G, Brandt H, Wertmer H & Finkelmann H 2009 *C. R. Chimie* **12**, 85–104.
Kundler I & Finkelmann H 1995 *Macromol. Rapid Commun.* **16**, 679–686.
Lehmann W, Skupin H, Tolksdorf C, Gebhard E, Zentel R, Krüger P, Lösche M & Kremer F 2001 *Nature* **410**, 447–450.
Lubensky T, Mukhopadhyay R, Radzihovsky L & Xing X 2002 *Phys. Rev. E* **66**, 011702–1–011702–22.
Malvern L 1969 *Introduction to the Mechanics of a Continuous Medium* Prentice-Hall, Inc. Englewood Cliffs, NJ.
Martinoty P, Stein P, Finkelmann H, Pleiner H & Brand H 2004 *Eur. Phys. J. E* **14**, 311–321.
Mayer S & Zentel R 2002 *Curr. Opin. Solid St. M.* **6**, 545–551.
P. de Gennes & Prost J 1993 *The Physics of Liquid Crystals* Oxford Science Publications Oxford.
McMeeking R & Landis C 2005 *J. Appl. Mech* **72**, 581–590.
Nishikawa E & Finkelmann H 1997 *Macromol. Rapid Commun.* **18**, 65–71.
Palffy-Muhoray P, Cao W, Moreira M, Taheri B & Munoz A 2006 *Phil. Trans. Roy. Soc. A* **364**, 2747–2761.
Rey A & Denn M 2002 *Annu. Rev. Fluid Mech.* **34**, 233–266.
Spillman C, Ratna B & Naciri J 2007 *Appl. Phys. Lett.* **90**, 021911–1–021911–3.
Su Y & Landis C 2007 *J. Mech. Phys. Solids* **55**, 280–305.
Suo Z, Zhao X & Greene W 2008 *J. Mech. Phys. Solids* **56**, 467–486.
Terentjev E 1993 *Europhys. Lett.* **23**(1), 27–32.
Terentjev E, Warner M & Verwey G 1996 *J. Phys. II France* **6**, 1049–1060.
Virga E 1994 *Variational theories for liquid crystals* Chapman & Hall London.
Viswanathan N, Kim D, Bian S, Williams J, Liu W, Li L, Samuelson L, Kumar J & Tripathy S 1999 *J. Mater. Chem.* **9**, 1941–1955.
Warner M, Gelling K & Vilgis T 1988 *J. Chem. Phys.* **88**, 4008–4013.
Warner M & Kutter S 2002 *Phys. Rev. E* **65**, 051707–1–051707–9.
Warner M & Terentjev E 2007 *Liquid Crystal Elastomers–Revised Edition* Oxford Science Publications Oxford.
Woltman S, Jay G & Crawford G 2007 *Nat. Mater.* **6**, 929–938.
Yu P, Hu S, Chen L & Du Q 2005 *J. Comput. Phys.* **208**, 34–50.
Zhang W & Bhattacharya K 2005 *Acta. Mater.* **53**, 185–198.
Zhao X, Hong W & Suo Z 2007 *Phys. Rev. B* **76**, 134113–1–134113–9.